Current Chemistry Letters 13 (2024) 655–668

Contents lists available at GrowingScience

Current Chemistry Letters

homepage: www.GrowingScience.com

Recognition of trivalent analytes using simple organic chromogenic and fluorogenic probes: A review

Duraisamy Udhayakumari[a*]

[a]*Department of Chemistry, Rajalakshmi Engineering College, Chennai – 602105, India*

C H R O N I C L E

Article history:
Received January 20, 2024
Received in revised form
March 21, 2024
Accepted May 14, 2024
Available online
May 14, 2024

Keywords:
Organic probes
Trivalent ions
Toxicity
Detection limit
Chemosensor
Applications

A B S T R A C T

Trivalent analytes such as Fe^{3+}, Cr^{3+} and Al^{3+} play pivotal roles in various fields including environmental monitoring, biological sensing, and industrial processes. The development of efficient and selective detection methods for trivalent species is therefore of paramount importance. In this review, we present an overview of recent advances in the recognition of trivalent analytes using simple organic chromogenic and fluorogenic probes. In this review we discuss the strategies employed for the design and synthesis of chromogenic and fluorogenic probes tailored for trivalent analytes, highlighting key structural motifs and functional groups that contribute to their recognition capabilities.

1. Introduction

Detecting and quantifying trivalent analytes is crucial in environmental monitoring, biological research, and industrial applications due to their widespread presence and impact. Trivalent ions, distinguished by their distinct chemical characteristics, serve essential functions in biological processes, catalytic reactions, and the synthesis of materials. Nonetheless, elevated levels of these analytes can lead to significant environmental and health hazards. [1-2] Researchers have been investigating various methods to tackle the complexities of trivalent analyte detection, spanning from conventional analytical methods to cutting-edge sensor technologies. Within this spectrum, the adoption of uncomplicated organic chromogenic and fluorogenic probes has surfaced as a viable strategy, offering simplicity, sensitivity, and adaptability. [3-5]

The field of recognizing trivalent analytes using simple organic chromogenic and fluorogenic probes has seen significant advancements. Researchers have developed various probes that exhibit high selectivity and sensitivity toward trivalent ions, such as Fe^{3+}, Al^{3+}, and Cr^{3+}. These probes function through mechanisms like photoinduced electron transfer (PET), intramolecular charge transfer (ICT), and coordination-induced fluorescence enhancement or quenching. The primary focus has been on creating cost-effective, easy-to-synthesize probes with potential applications in environmental monitoring, biomedical diagnostics, and industrial processes. Recent studies emphasize enhancing probe performance by improving detection limits, response times, and stability in diverse environments[6-7].

This review seeks to offer a thorough examination of the latest progressions in trivalent analyte detection using organic chromogenic and fluorogenic probes (**Table 1**). It will delve into the core principles governing the design and operation of these probes, their selectivity for particular trivalent analytes, and their potential uses across different fields. Through an analysis of recent advancements and hurdles in this swiftly evolving domain, this review aims to provide valuable insights to steer future research endeavors towards the creation of reliable and effective detection systems for trivalent analytes.[7-13]

* Corresponding author
E-mail address udayakumari.d@rajalakshmi.edu.in (D. Udhayakumari)

doi: 10.5267/j.ccl.2024.6.001

2. Trivalent ions detection using simple organic probes

2.1 Chemosensors for Fe^{3+} ion detection

A novel fluorescence receptor, R1, based on imidazole, has been developed for the selective and sensitive detection of Fe^{3+} in DMSO medium.[14] When used in polar protic solvents like MeOH and EtOH, R1 exhibited decreased emission. This reduction in emission is attributed to the interaction between imidazole and alcohol molecules, causing quenching due to hydrogen bonding. Specifically, hydrogen bonds formed between the imidazole ring and the oxygen atom of alcohol, as well as between the nitrogen atom of the oxime group and the hydrogen atom of alcohol, interrupt the ESIPT (Excited-State Intramolecular Proton Transfer) mechanism. Conversely, in polar aprotic solvents such as DMSO, EtOAc, THF, and $CHCl_3$, the emission intensity of R1 significantly increased. In the absence of Fe^{3+}, the receptor R1 displayed its highest emission band at 509 nm. However, upon the addition of Fe^{3+} to R1, fluorescence emission quenching was observed (**Fig. 1**).

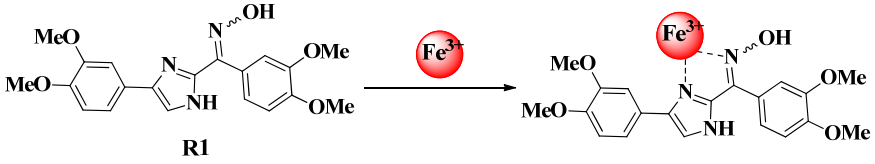

Fig. 1. Structure of R1

A receptor named R2, based on benzimidazole, specifically 2-(1H-Benzimidazol-2-yl) phenol, has been synthesized through a three-component cyclization reaction.[15] This receptor has been reported for its selective and sensitive detection of Fe^{3+} in ethanol. In ethanol medium, R2 exhibits an emission band at 337 nm with a quantum yield of 0.63. Upon the introduction of Fe^{3+}, the emission peak at 337 nm gradually decreases to 0.02, with a detection limit of 0.5 µM. Moreover, dual emission has been observed for receptor R2, attributed to excited-state intramolecular proton transfer in the presence of an aprotic solvent. The presence of Fe^{3+} results in the formation of R2- Fe^{3+} (in a 2:1 ratio), which subsequently undergoes a structural change. This change causes the phenol O-H of R2 to undergo tautomerism to C=O, leading to fluorescence quenching. Interestingly, reversible fluorescence emission enhancement is observed upon the addition of H_3PO_4 into R2-Fe^{3+} due to the deactivation of the complex (**Fig. 2**).

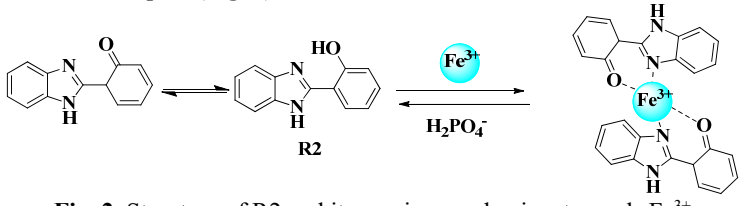

Fig. 2. Structure of R2 and its sensing mechanism towards Fe^{3+}

A newly developed fluorescent receptor, denoted as R3, featuring a quinoline-appended benzimidazole motif, has been devised and documented for its proficiency in identifying Cu^{2+} and Fe^{3+} ions in Tris-HCl buffer (50 mM, pH 7.2).[16] Under excitation at 370 nm, receptor R3 exhibited a robust emission peak in the green spectrum at 508 nm. Upon introduction of various metal ions into R3, only Cu^{2+} and Fe^{3+} ions demonstrated a significant reduction in emission intensity, indicative of their distinctive quenching behavior. This quenching phenomenon can be attributed to the chelation-enhanced fluorescence quenching (CHEQ) effect induced by paramagnetic Cu^{2+} and Fe^{3+}. The detection limit for R3 towards Cu^{2+} and Fe^{3+} was determined to be 13µM and 12µM, respectively. Furthermore, the binding constant and binding stoichiometry were calculated to be 8.6×10^4 M^{-1} and 1:1, respectively. Notably, the sensing mechanism of receptor R3 allows for cellular permeability and holds promise for fluorescence imaging of Cu^{2+} and Fe^{3+} species within living cells (Figure. 3).

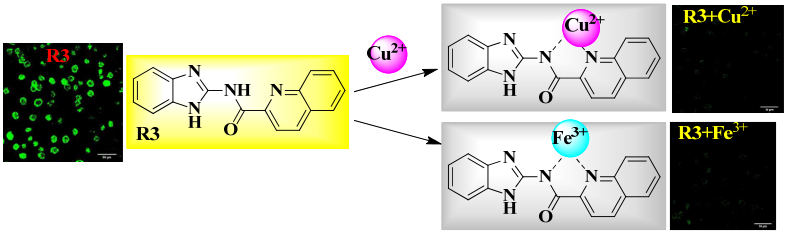

Fig. 3. Structure of R3

A newly synthesized receptor, named R4, featuring a quinoline-functionalized Schiff-base derivative, was developed and characterized. R4 exhibited remarkable selectivity and sensitivity in detecting Fe^{3+} ions in a DMSO/H_2O solution (3:7, v:v; HEPES buffered, pH 7.2).[17] Initially, R4 displayed weak fluorescence emission at 500 nm. However, upon the addition of various metal ions, including Ca^{2+}, Mg^{2+}, Ni^{2+}, Al^{3+}, Cu^{2+}, Hg^{2+}, Zn^{2+}, Ba^{2+}, Co^{2+}, K^+, Na^+, Ag^+, Fe^{3+}, Cr^{3+}, Cd^{2+}, and

Pb^{2+}, only Fe^{3+} showed significant fluorescence enhancement at 500 nm, accompanied by a red shift to 510 nm. This fluorescence enhancement phenomenon was attributed to the chelation-enhanced fluorescence (CHEF) effect induced by the interaction between R4 and Fe^{3+}. The binding mode between R4 and Fe^{3+} occurred in a 1:1 ratio, with a calculated detection limit of 4.3 nM. Furthermore, the introduction of PPi into the R4-Fe^{3+} complex resulted in enhanced fluorescence, indicating the decomplexing of Fe^{3+} in the presence of PPi. Utilizing the Fe^{3+} displacement approach, the detection limit for PPi was determined to be 8.2×10^{-8} M (**Fig. 4**).

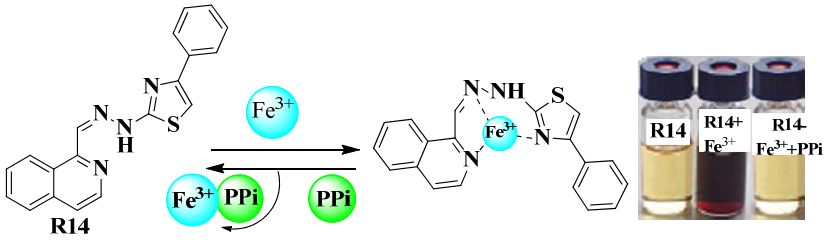

Fig. 4. Sensing mechanism R4 towards Fe^{3+} and its chromogenic changes

A straightforward fluorescence-based receptor R5, has been developed for the specific and sensitive detection of Fe^{3+} ions in a CH_3CN/H_2O (95/5, v/v) solvent mixture.[18] Upon the addition of Fe^{3+} ions to R5, a decrease in absorbance at 239 nm and appearance of a band at 251 nm were observed, with an isosbestic point at 243 nm, indicating the formation of a Fe^{3+} complex. Additionally, a new broad band around 350 nm, extending to 400 nm, further confirmed the complex formation. The inherent strong fluorescence of free receptor R5 was attributed to the inhibition of the excited-state intramolecular proton transfer (ESIPT) process. Upon increasing Fe^{3+} concentration, a significant fluorescence quenching at 400 nm and emergence of a new broad emission band around 500 nm were observed in the fluorescence emission spectrum, suggesting a strong interaction between receptor R5 and Fe^{3+} ions through the metal-to-ligand charge transfer (MLCT) effect. This fluorescence quenching and red-shifted fluorescence were attributed to the hydrogen bond-induced intramolecular excited-state proton transfer process. The detection limit and binding mode of receptor R5 were determined to be 2.8 µM and 1:1 stoichiometry, respectively (**Fig. 5**).

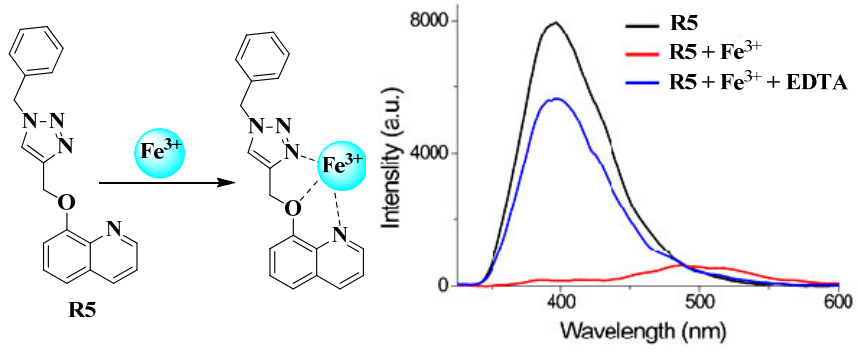

Fig. 5. Structure of R5 and its sensing mechanism towards Fe^{3+}

A novel receptor R6 and based on 8-hydroxyquinoline, has been introduced for the colorimetric and fluorescence detection of Fe^{3+} ions in ethanol-water (1:99, v/v) solution.[19] When exposed to 30 different metal ions (with excitation at 350 nm), R6 exhibited minimal fluorescence emission on its own. However, significantly enhanced fluorescence intensity at 480 nm was observed upon the addition of Al^{3+} ions. In the presence of Fe^{2+} and Fe^{3+} ions, R6 displayed a distinct color change from yellow to black, accompanied by additional peaks at 371, 460, and 580 nm. This property renders R6 capable of serving as a colorimetric sensor for the 'naked eye' detection of Fe^{3+} and Fe^{2+} ions. The calculated detection limits were 7.38 µM, 42.4 µM, and 56 µM for Al^{3+}, Fe^{2+}, and Fe^{3+}, respectively. Moreover, R6 demonstrated potential for the simultaneous recognition of the three metal cations (Al^{3+}, Fe^{3+}, and Fe^{2+}). The binding mode between R6 and Fe^{2+}/Fe^{3+} was determined to be 1:1 stoichiometry (**Fig. 6**).

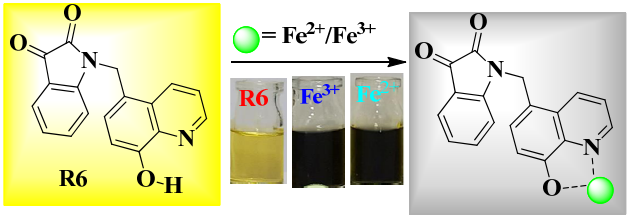

Fig. 6. Structure of R6 and its sensing mechanism towards Fe^{3+}/ Fe^{2+}

A newly developed quinoline-based receptor, named R7, specifically 1, 3-dioxoisoindolin-2-yl quinoline-2-carboxylate, has demonstrated remarkable fluorescence sensing capabilities for Fe^{3+} ions in a DMSO:H_2O mixture (8:2, v/v).[20] This chemosensor exhibited high selectivity and sensitivity, showing a distinct "on-off" fluorescence response upon interaction with Fe^{3+}. Upon excitation at 340 nm, receptor R7 emitted strong fluorescence at 400 nm. However, upon addition of Fe^{3+} ions to R7, a significant fluorescence quenching was observed, attributed to the more paramagnetic nature of Fe^{3+} ions. The binding constant, stoichiometry, and detection limit of R7 with Fe^{3+} were determined to be $0.71\times10^2 M^{-1}$, 1:1, and 0.9-1.6 nM, respectively (**Fig. 7**).

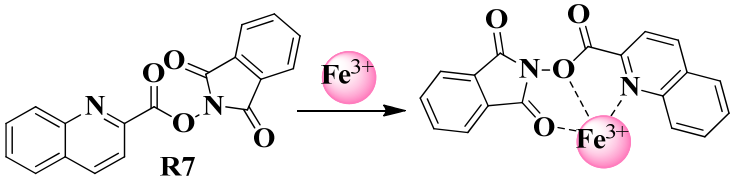

Fig. 7. Structure of R7 and its sensing mechanism towards Fe^{3+}

A fluorescence receptor, designated as R8, featuring a 1,2,3-triazole linkage with 8-hydroxyquinoline, has been developed for dual detection of Zn^{2+} and Fe^{3+} ions in a CH_3CN/H_2O binary solvent mixture.[21] R8 exhibited weak fluorescence in protic solvents like water, whereas it displayed strong fluorescence in non-protic solvents such as CH_3CN. Notably, R8 showed a more than 100 nm red shift in fluorescence response in protic solvents compared to non-protic solvents, potentially indicating involvement of intermolecular photoinduced proton transfer (PPT) processes with water molecules. In a CH_3CN/H_2O (5/95, v/v) solvent mixture, R8 functioned as a selective "turn-on" fluorescence sensor for Zn^{2+} ions and a selective "turn-off" fluorescence sensor for Fe_{3+} ions (with an 81 nm red shift). Upon coordination with Zn^{2+}, R8-Zn^{2+} complexes exhibited a blue-shifted fluorescence enhancement (62 nm) at 428 nm, attributed to the inhibition of intermolecular photoinduced proton transfer processes upon chelation with Zn^{2+}. The binding stoichiometry and detection limits of R8 with Zn^{2+} and Fe^{3+} ions were determined to be 1:1, with values of 0.99 μM (for Zn^{2+}) and 1.23 μM (for Fe^{3+}), respectively (Figure. 8).

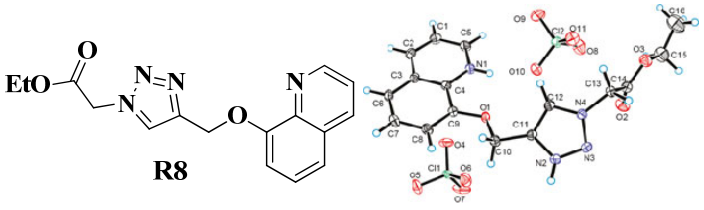

Fig. 8. Structure of R8

2.2 Chemosensors for Cr^{3+} ion detection

Novel bis-imidazol-phenol-dyes comprising three fluorescence receptors, namely R9a-c, were synthesized and designed for the fluorescence turn-on detection of Cr^{3+} ions in CH_3CN, operating through the ESIPT mechanism.[22] Upon introduction of various metal ions including Li^+, Na^+, K^+, Ca^{2+}, Cr^{3+}, Al^{3+}, Cd^{2+}, NH^{4+}, Zn^{2+}, Ag^+, Cu^{2+}, Ni^{2+}, Co^{2+}, Mn^{2+}, and Fe^{3+}, a distinctive blue-shifted emission band at approximately 407 nm (for R9a & c) and 396 nm for R9c, accompanied by notably high emission intensity, was solely observed in the presence of Cr^{3+} ions. This blue-shifted enhanced emission (turn-on effect) confirms the ESIPT capabilities of the fluorophores (R9a & c), which are activated by the inhibition of ESIPT in the presence of chromium ions. Job's plot studies revealed a binding mode of 2:1 between R9c and Cr^{3+} ions (**Fig. 9**).

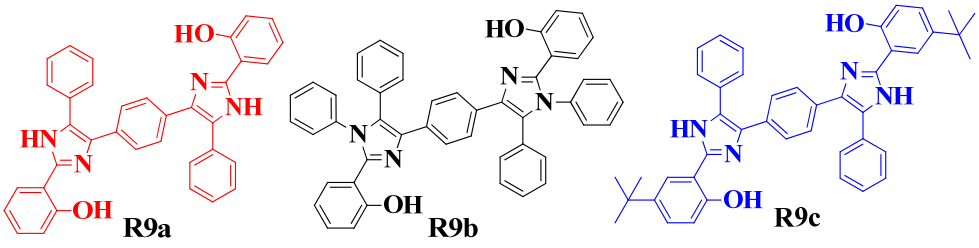

Fig. 9. Structure of R9a-c

Receptor R10 has been synthesized from Triphenylamine-Thiophenegroups coupling and employed for assessing the concentration of Cr^{3+} ions in an aqueous medium.[23] The unfettered fluorescent moiety exhibited robust emission at 530 nm, particularly prominent in THF compared to other solvents. Upon the addition of Cr^{3+}, a significant increase in fluorescent emission, 59 times higher than that of the metal-free moiety, was observed. This enhancement suggests the potential suitability of R10 for detecting Cr^{3+}. The introduction of Cr^{3+} inhibited the PET effect by restricting the movement of electrons from donor to acceptor within the receptor. Additionally, the formation of a Saxon blue color upon complex

formation further suggests the binding mechanism. R10 displayed high selectivity towards Cr^{3+} ions with no interference from other metal ions. The limit of detection (LOD) for Cr^{3+} ions was determined to be 1.5μM (**Fig. 10**).

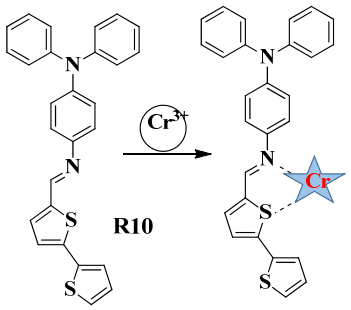

Fig. 10. Structure of fluorescence R10 with Cr^{3+}

Chalmareli et al. developed a novel fluorescence receptor R11, based on Schiff base chemistry, specifically designed for detecting Cr^{3+} ions in polar aprotic acetonitrile-water (95/5%).[24] Receptor R11 demonstrated a notable affinity for Cr^{3+} ions, as evidenced by fluorescence spectral studies. Upon addition of Cr^{3+} ions to receptor R11, the increasing concentration resulted in an emission spectrum peaking at 663 nm, indicating the inhibition of the photo-induced electron transfer process during complex formation (Figure. 11). This suggests that receptor R11 functions effectively as a sensor for Cr^{3+} ions. The calculated detection limit for R11 was determined to be $1.3x10^{-7}$ mol/L .

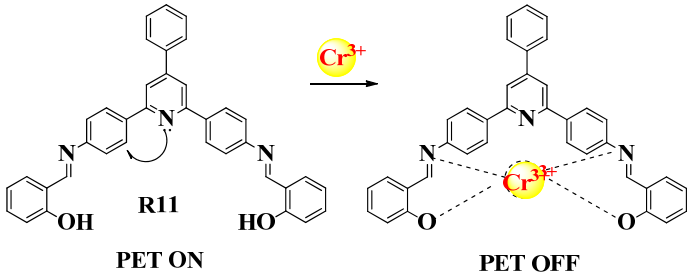

Fig. 11. Structure of R11 and metal binding mechanism

Zhang et al. developed a fluorescent receptor, R12, designed to detect Cr^{3+} ions, drawing from insights gained in previous studies. By incorporating a Schiff base compound, they enhanced the sensitivity of R12 towards Cr^{3+} ions.[25] Upon introduction of Cr^{3+} ions, a noticeable color change was observed by the naked eye, indicating successful binding. UV-visible spectral analysis further confirmed the interaction between Cr^{3+} ions and receptor R12, showing a reduction in absorption peak (<447nm) compared to the base peak of R12. The binding mechanism was elucidated through several observations, including proton peak shifting in the imine group, the absence of intramolecular hydrogen bonding in the naphthalene ring, and the involvement of an oxygen atom from the carboxylic acid group of the benzene ring in R12. The detection limit was determined to be 3.37×10^{-7} M, with a calculated binding constant of 2.06×10^{6} for Cr^{3+} ions, derived from the Benesi Hildebrand equation (**Fig.12**).

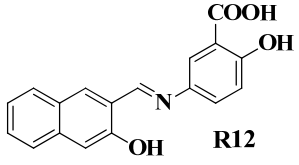

Fig. 12. Chemical Structure of R12

Vijayakumar and his colleagues designed receptor R13, a simple organic molecule, specifically for detecting Cr^{3+} ions in aqueous environments.[26] When treated with Cr^{3+} ions, the color of R13 changed noticeably. The receptor R13 solution exhibited yellow color to colorless solution in the naked eye under UV–Vis lamp. The receptor R13 solution demonstrated a strong absorption band around 284 nm observed due to π- π* electronic transition with detection of Cr^{3+} and without any interference by other metal ions. The addition of Cr^{3+} ions to R13 resulted in a strong fluorescence emission peak at 428 nm, and even with a visual fluorescence change from light yellow to light blue. Investigation into the binding mechanism revealed that the interaction between receptor R13 and Cr^{3+} ions restricted free-electron transfers from the -C=N group to the -NH group, leading to a quenched PET process. These findings indicate that receptor R13 exhibits promising selectivity towards Cr^{3+} ions (**Fig. 13**).

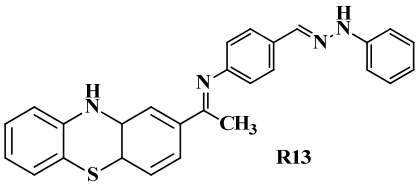

Fig. 13. Chemical structure of R13

Kolcu et al. synthesized two fluorescent receptors, 14a and 14b, from two salicylaldimine derivatives, specifically designed for detecting Cr^{3+} ions.[27] In receptor 14a, the intense emission observed at 530 nm is attributed to the ICT process. However, upon addition of Cr^{3+} ions, a new emission band emerged at 508 nm due to the blocking of the ICT process caused by the formation of a complex between Cr^{3+} ions and receptor 14a. In contrast, receptor 14b exhibited weak emissions centered at 490 nm, attributed to ESIPT reflection and the isomeric effect of functional groups. The addition of Cr^{3+} ions resulted in intensified emission, attributed to the "ON" CHEF effect and inhibited PET effect. Consequently, receptors 14a and 14b demonstrate enhanced sensitivity in the "ON-OFF" PET fashion. Titration experiments revealed a 2:2 stoichiometry ratio for the interaction between receptors 14a and 14b with Cr^{3+} ions (**Fig. 14**).

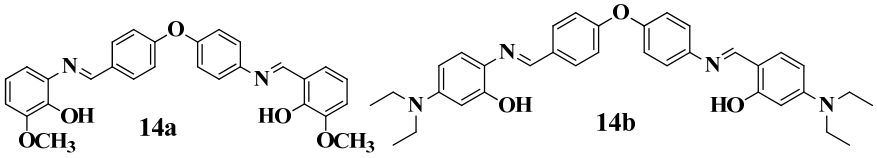

Fig. 14. Chemical structure of R14a-b

Dinesh Kumar et al. developed receptor R15 using a novel Schiff base fluorescent moiety to achieve sensitive detection of Cr^{3+} ions at low levels.[28] A stock solution of receptor R15 was prepared in DMF:H_2O (4:1, v/v), and upon addition of Cr^{3+} ions, a quenched fluorescence was observed. This quenching effect is attributed to the formation of a bond between the metal ion and the active center of the sensor, inhibiting the PET process. Receptor R15 demonstrated a detection limit of 0.5 µM for Cr^{3+} ions. To underscore the selectivity of receptor R15 for Cr^{3+} ions, in vitro studies were conducted on both empty HepG2 cells and HepG2 cells cultivated with receptor R15 and Cr^{3+} ions. The fluorescence was switched off in the presence of Cr^{3+} ions, confirming the role of receptor R15 in detecting chromium ions in living cells (**Fig. 15**).

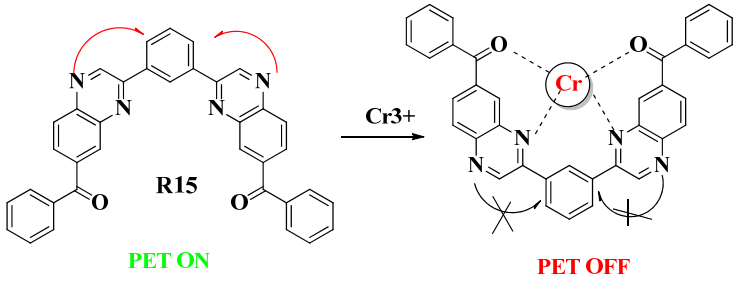

Fig. 15. Structure of fluorescence receptor R15 and its binding mechanism

Hu et al. developed a novel fluorescent receptor, R16, consisting of a naphthalene derivative ring connected to a fluorophore via a -C= N bond.[29] In CH_3CN-H_2O (v/v, 7:3), receptor R16 exhibited weak emission at 305 nm in the absence of Cr^{3+} ions, but upon their addition, a significant fluorescence enhancement (923 times) was observed. The fluorescence enhancement in receptor R16 is attributed to the formation of a complex with Cr^{3+} ions, followed by oxidation facilitated by the unstable C–N–O three-membered ring structure, leading to the formation of an amide group and subsequent arrest of cis-trans isomerization of the imine group. Receptor R16 demonstrated a low detection limit of 63.1 nM for Cr^{3+} ions (Figure. 16).

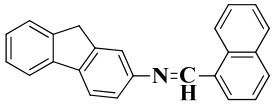

R16

Fig. 16. Chemical structure of R16

Mukherjee et al. aimed to develop receptor R17 using a pyrene-based luminescent compound for detecting Cr^{3+} ions.[30] In the absence of ions, receptor R17 exhibited weak fluorescence with a quantum yield (Φ) of 0.035. However, upon the addition of Cr^{3+} ions, fluorescence enhancement was observed, attributed to Chelation-enhanced fluorescence by pyrene (a 4.3 times increase) in DMSO. For the first time, Derivative Synchronous Fluorescence Spectroscopy (DSFS) was employed

to investigate the relationship between receptor R17 and Cr^{3+} ions. The limit of detection (LOD) was determined to be 4.925×10^{-9} M with a limit of quantification of 1.64×10^{-8} M, and a stoichiometry relation of 2:1 was established (**Fig. 17**).

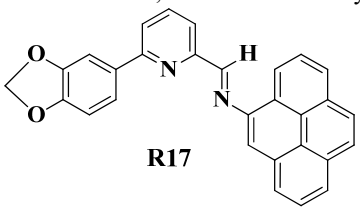

Fig. 17. Chemical structure of R17

A novel receptor, R18, was developed by combining two simple molecules, proving to be an effective sensor not only for Cr^{3+} ions but also for other trivalent cations.[31] When tested alone, receptor R18 exhibited weak emission. However, upon the addition of Cr^{3+} ions in an aqueous medium, remarkable fluorescence enhancement was observed along with a noticeable color change. The formation of complexes within receptor R18 with the assistance of Cr^{3+} ions inhibited the PET effect and induced CHEF. The stoichiometry ratio between receptor R18 and Cr^{3+} ions was determined to be 1:1. Impressively, receptor R18 demonstrated a remarkably low detection range of 1.15 µM. In biological assays, it exhibited low cytotoxicity and enabled the detection of Cr^{3+} ions in HDF cells (Figure. 18).

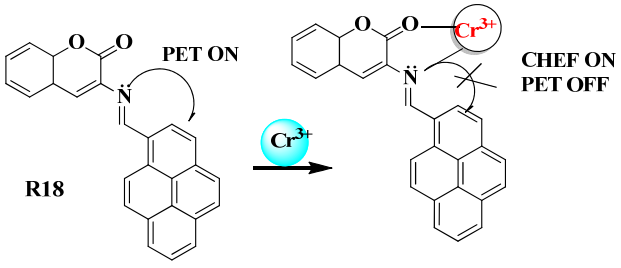

Fig. 18. Structure of fluorescence receptor 18 and binding its mechanism towards Cr^{3+}

2.3 Chemosensors for Al^{3+} ion detection

A novel fluorescent receptor, R19, serves as an efficient sensor for detecting Al^{3+} ions in DMF/H_2O (1/9, v/v, pH = 7.4, 0.01 M HEPES) among a range of other metal ions.[32] Due to the dominant decay process involving the isomerization of the C=N moiety and the ESIPT process, receptor R19 exhibits weak fluorescence at 506 nm. However, upon the addition of Al^{3+} ions, a significant enhancement in fluorescence at 496 nm was observed. This enhancement is attributed to the inhibition of C=N isomerization and the ESIPT process upon coordination of receptor R19 with Al^{3+}. The detection limit was calculated to be 0.48 nM based on fluorescence spectrum and 8.47 nm based on absorption spectrum (**Fig. 19**).

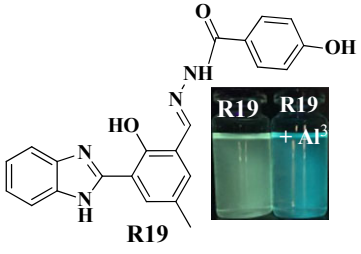

Fig. 19. Structure of R19

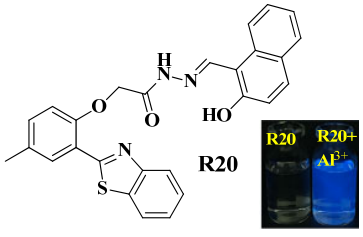

Fig. 20. Structure of R20

S. Zeng and colleagues introduced a novel receptor, R20, which utilizes naphthaldehyde-conjugated benzothiazole for selective and sensitive detection of Al^{3+} in a DMF/H_2O (v/v, 4/6) solution.[33] This probe operates with a binding mode of 1:1 and exhibits a detection limit ranging from 0.056 to 0.509 nM. In the presence of Al^{3+} ions, receptor R20 demonstrates significant fluorescence enhancement at 465 nm (with a quantum yield of 0.82) under an excitation wavelength of 365 nm. Notably, under UV light at 365 nm, receptor R20 undergoes a color change from colorless to bright blue upon interaction with Al^{3+} ions. The observed fluorescence enhancement (within a pH range of 4-7) is attributed to the inhibition of the ESIPT processes and C=N isomerization. Furthermore, the practical utility of receptor R20 extends to quantifying Al^{3+} levels in real water samples, implementing logic gates, and conducting bioimaging in human stromal cells (**Fig. 20**).

A newly developed fluorescence receptor, R21, has been introduced as a highly selective and sensitive sensor for detecting Al^{3+} ions in a solution composed of H_2O/MeOH (9/1, v/v), along with 10 mM PBS buffer at pH 7.3 and 25°C.[34]

Initially, the free receptor R21 exhibits two emission bands at 435 nm and 565 nm. Upon the addition of Al^{3+} ions, the color of receptor R21 shifts from colorless to light yellow. Subsequently, the intensity of the emission band at 565 nm decreases while a new band emerges at 480 nm. This alteration in fluorescence color from red to cyan results from the inhibition of ESIPT. Intramolecular hydrogen bonds between phenolic –OH and the hydrazide linker, as well as between phenolic –OH and the –N atom of the benzothiazole system, have been confirmed through single crystal XRD studies. Upon interaction with Al^{3+} ions, a stable complex forms between the receptor R21 and the ion, leading to the inhibition of ESIPT. The association constant, stoichiometry, and detection limit were determined to be 1.24×10^5 M^{-1}, 1:1, and 0.672 nM, respectively (**Fig. 21**).

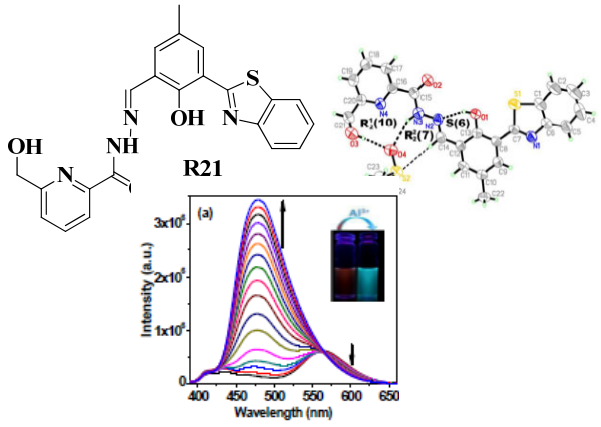

Fig. 21. Structure of R21

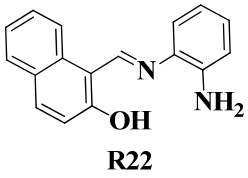

Fig. 22. Structure of R22

A novel fluorescence sensor, R22, has been devised utilizing the excited state intramolecular proton transfer (ESIPT) and twisted intramolecular charge transfer (TICT) mechanism for detecting Al^{3+} ions.[35] The ESIPT product, characterized by a lower potential energy, is crucial in this design, with an energy barrier for the ESIPT process precisely measured at 10.2 kJ/mol. Initially, receptor R22 exhibits a weak emission peak at 499 nm, originating from the ESIPT product. Upon coordination with Al^{3+} ions, which bind to the nitrogen and oxygen atoms (Lewis bases) on receptor R22, the original charge transfer process is impeded. Consequently, a significant fluorescence enhancement is observed at 473 nm. This fluorescence turn-on is attributed to the removal of the original energy barrier for the ESIPT process, rendering it barrier-less, while the formation of an organometallic compound prohibits the TICT process (**Fig. 22**).

` A fluorescence receptor, R23, selective for Al^{3+} ions and derived from naphthalene, has been developed based on both excited state intramolecular proton transfer (ESIPT) and photoinduced electron transfer (PET) mechanisms.[36] Upon interaction with Al^{3+} ions, the absorption spectrum of the receptor reveals a gradual decrease in bands at 325 nm and 366 nm, with a new absorption band emerging at 432 nm. Initially, the receptor exhibits weak fluorescence emission at 475 nm (with a quantum yield of 0.5%) upon excitation at 415 nm. However, only the addition of Al^{3+} ions results in a notable enhancement of fluorescence emission at 475 nm (with a quantum yield of 26.4%). The detection limit for the R23-Al^{3+} complex is determined to be 0.43 μM, with a stoichiometry of 1:1 (**Fig. 23**).

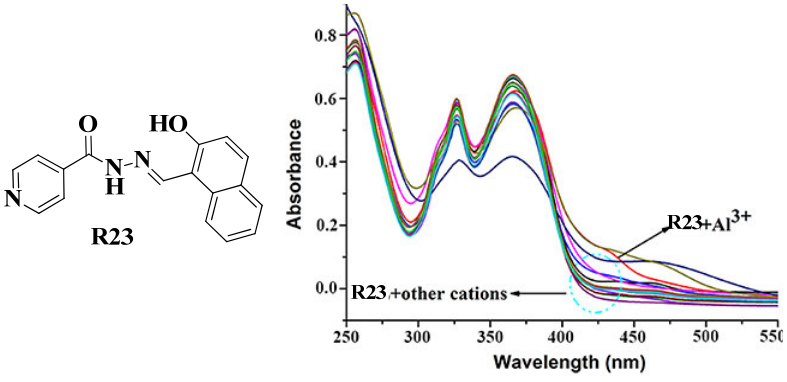

Fig. 23. Structure of R23

A newly designed naphthalimide-based receptor, R24, has been synthesized for the ratiometric detection of Al^{3+} ions by inhibiting excited state intramolecular proton transfer (ESIPT) in a solution comprising H_2O/CH_3CN (1:9; v/v).[37] The absorption spectrum of R24 exhibits two distinct charge transfer bands at 340 nm and 460 nm. Upon excitation at 460 nm,

the receptor displays emission bands at 510 nm and 610 nm. Upon interaction with Al^{3+} ions, R24 undergoes a color change from orange to yellow, accompanied by a ratiometric increase in the charge transfer band at 460 nm. Additionally, under UV light, the R24-Al^{3+} complex emits blue-green light, with an enhanced emission band observed at 540 nm. The receptor also demonstrates ratiometric detection of F- ions, manifesting a color change from orange to purple and emitting light at 570 nm. The calculated detection limits for receptor R24 with Al^{3+} and F^- ions are 32 nM and 75 µM, respectively (**Fig. 24**).

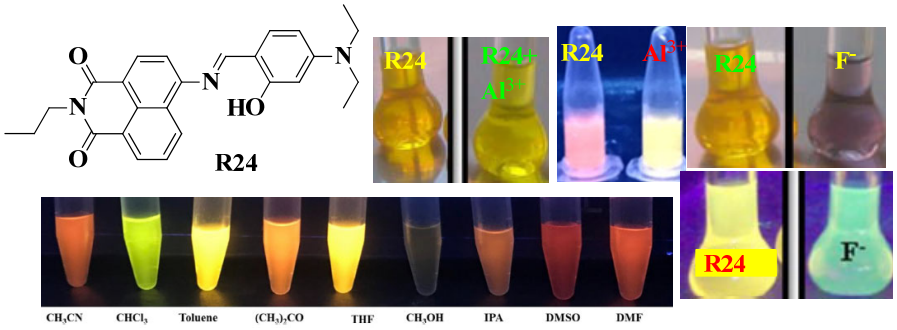

Fig. 24. Structure of R24 and its visual and fluorescence color change

A fluorescence receptor, R25, designed for detecting aluminium ions (Al^{3+}) based on excited state intramolecular proton transfer (ESIPT), has been synthesized and its binding properties investigated in a CH_3CN-H_2O medium (9:1 v/v).[38] Upon excitation at 445 nm, the receptor exhibits an intense emission band at 445 nm, indicating a large Stokes shift. In acetonitrile, the receptor displays a bright cyan color with an emission band at 445 nm. Upon addition of aluminium ions to R25, the bright cyan color transforms into deep blue, accompanied by enhanced fluorescence emission at 412 nm. The detection limit and binding mode for R25-Al^{3+} interaction were determined to be 0.5 nM and 1:1, respectively (**Fig. 25**).

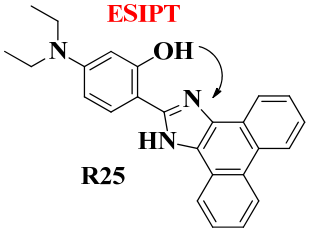

Fig. 25. Structure of R25

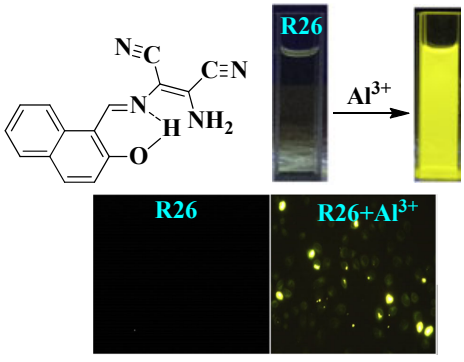

Fig. 26. Structure of R26

A fluorescence receptor, R26, tailored for selective detection of Al^{3+} ions, has been synthesized and documented. Initially, the receptor exhibits very weak emission at 556 nm, attributed to isomerization around the C=N linkage.[39] Upon interaction with Al^{3+} ions, R26 displays dual-channel emission at 522 nm and 558 nm, emitting yellow fluorescence. This fluorescence enhancement is credited to the inhibition of C=N and photoinduced electron transfer (PET) isomerization post-binding with Al^{3+}. The dual emissions arise from intramolecular charge transfer (ICT) and excited state intramolecular proton transfer (ESIPT) processes. The binding constant, stoichiometry, and detection limit for the R26-Al^{3+} complex were determined as 9.55×10^8 M^{-2}, 1:2, and 10.2 nM, respectively. Notably, based on bioimaging studies, R26 exhibits promise in detecting intracellular Al^{3+} in living cells (**Fig. 26**).

A fluorescent receptor labeled as R27, composed of carbazole-conjugated Schiff base, has been devised for detecting Al^{3+} ions in an ethanol-water (1:1, v/v) medium.[40] Upon interaction with the metal ions, the receptor exhibits a new absorption band at 531 nm, attributed to the transfer of lone pairs of electrons from the nitrogen/oxygen atoms of the receptor to the metal ion. Initially, the receptor displays weak fluorescence emission, stemming from isomerization of the C = N bond in the excited state through excited state intramolecular proton transfer (ESIPT). However, in the presence of Al^{3+} ions, an intensified fluorescence emission is observed due to the disturbance of the ESIPT process. The association constant, binding mode, and detection limit of receptor R27 with Al^{3+} were determined as 5×10^4 M^{-1}, 1:1, and 2.59 µM, respectively (**Fig. 27**). A novel fluorescence receptor, R28, featuring a Schiff base design, specifically (E)-4-methyl-2-((2-(9-(naphthalen-1-yl)-8-(thiophen-2-yl)-9H-purin-6-yl)hydrazono)methyl)phenol, has been developed and disclosed for the detection of Al^{3+} ions in a DMSO/H_2O (9/1, v/v, pH = 7.4) environment.[41] Initially non-fluorescent, the receptor exhibits intensified emission intensity at 462 nm and 488 nm upon interaction with Al^{3+} ions. This enhancement in fluorescence emission of receptor R28 is likely attributed to the suppression of photoinduced electron transfer (PET) and excited state

intramolecular proton transfer (ESIPT) processes induced by Al^{3+}. The detection limit and binding mode of R28 were determined to be 82 nM and 1:1, respectively. Notably, R28 demonstrates efficient detection of trace amounts of Al^{3+} in test strips and living HeLa cells (**Fig. 28**).

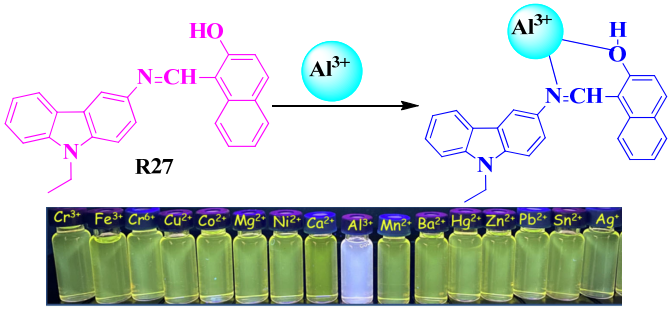

Fig. 27. Structure of R27 and its sensing mechanism towards Al^{3+}

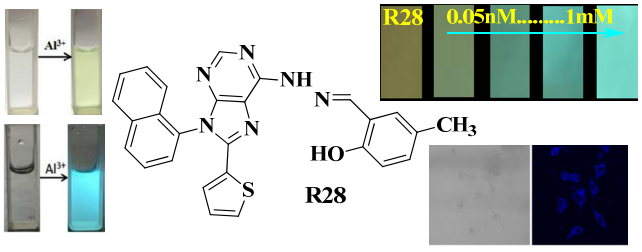

Fig. 28. Structure of R28 and its fluorescence images

A highly effective fluorescence receptor, designated as R29, has been synthesized through the combination of Bis(2-aminophenyl) ether and salicylaldehyde.[42] The receptor's structural characteristics have been thoroughly elucidated through FTIR, ^{1}H NMR, ^{13}C NMR, and mass spectroscopic analyses. Upon the introduction of Al^{3+} ions to R29, a significant fluorescence enhancement occurs, reaching 528-fold at a wavelength with a large Stokes shift. This fluorescence enhancement is attributed to the presence of electron-releasing substituents on the phenol rings, facilitating an excited state intramolecular proton transfer (ESIPT) mechanism. The detection limit and stoichiometry of R29 with Al^{3+} ions were determined to be 5.48 nM and a 1:1 binding mode, respectively (**Fig. 29**).

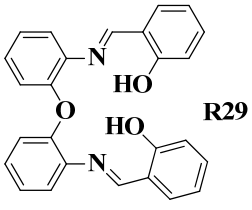

Fig. 29. Structure of R29

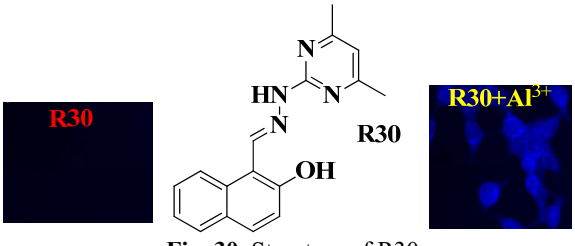

Fig. 30. Structure of R30

Receptor R30, synthesized from hydrazine pyrimidine, specifically (1-[(4,6-Dimethyl-pyrimidin-2-yl)-hydrazonomethyl]- naphthalen-2-ol), was developed using 2-hydroxy-1-naphthaldehyde and 4,6-dimethyl-2-hydrazinopyrimidine.[43] Its ability to detect Al^{3+} ions was assessed in an ethanol solution with 20 μM HEPES buffer at pH 7.2. Upon the addition of Al^{3+} ions to R30 (initial quantum yield $\Phi = 0.0066$), a significant increase in fluorescence emission was observed at 475 nm ($\Phi = 0.0955$). This enhanced fluorescence may be attributed to charge transfer, excited state intramolecular proton transfer (ESIPT), and the inhibition of photoinduced electron transfer (PET) phenomena. Additionally, under UV light, a distinct bright greenish-blue fluorescence was observed. The association constant, stoichiometry, limit of detection (LOD), and limit of quantification (LOQ) for the R30-Al^{3+} interaction were estimated to be 1.9×10^{4}, 1:1, 2.78 μM, and 9.27 μM, respectively (**Fig. 30**).

Table 1. Summary of simple organic probes based chromogenic and fluorogenic Fe^{3+}, Cr^{3+} and Al^{3+} ions detection

Sensor Number	Functional group	Method	Sensing ions	Solvent medium	Stoichiometry	LOD	Applications	Reference No
R1	Imidazole	Fluorogenic	Fe^{3+}	DMSO, MeOH, EtOH, $CHCl_3$, THF, EtOAc	1:1	-	-	14
R2	Benzimidazole	Fluorogenic	Fe^{3+}	Ethanol	1:2	0.5 µM	-	15
R3	Quinoline	Fluorescence	Cu^{2+} and Fe^{3+}	Tris-HCl buffer	1:1	12µM	Bioimaging studies	16
R4	Quinoline	Colorimetric & Fluorescence	Fe^{3+}	DMSO-H_2O	1:1	4.3 nM	-	17
R5	Quinoline	Fluorescence	Fe^{3+}	CH_3CN-H_2O	1:1	2.8 µM	-	18
R6	Quinoline	Colorimetric & Fluorescence	Fe^{3+} Fe^{2+} Al^{3+}	Ethanol-water	1:1	56 µM 42.4 µM 7.38 µM	-	19
R7	Quinoline	Fluorescence	Fe^{3+}	DMSO-H_2O	1:1	0.9-1.6 nM	-	20
R8	Quinoline	Fluorescence	Zn^{2+} and Fe^{3+}	CH_3CN-H_2O	1:1	0.99 µM (Zn^{2+}) and 1.23 µM (Fe^{3+})	-	21
R9	Imidazole	Fluorogenic	Cr^{3+}	CH_3CN	2:1	-	-	22
R10	Triphenylamine	Colorimetric/ Fluorescent	Cr^{3+}	Water	1:1	1.5 µM	-	23
R11	Schiff base	Fluorescent	Cr^{3+}	CH_3CN-H_2O	1:1	13 µM	-	24
R12	Schiff base	Colorimetric	Cr^{3+}	DMF	1:1	33 µM	-	25
R13	Schiff base	Colorimetric/ Fluorescent	Cr^{3+}	EtOH	1:1	86 µM	Cytotoxicity, Living cell imaging	26
R14	Schiff base	Colorimetric/ Fluorescent	Cr^{3+}	CH_3CN		11 µM (5a) 77 µM (5b)	Tap water samples, Colorimetric test-kits	27
R15	Schiff base	Colorimetric/ Fluorescent	Cr^{3+}	DMF/H_2O= 4/1, v/v,10MmHEPES buffer, pH= 7.0	1:1	0.5 µM	Living cell imaging	28
R16	Schiff base	Fluorescent	Cr^{3+}	CH_3CN-H_2O (v/v, 7:3).	1:1	63.1 nM	Real sample studies	29
R17	Pyrene	Colorimetric/ Fluorescent	Cr^{3+}	DMSO/H_2O (2:1) at 298 K.	2:1	49 nM	-	30
R18	Pyrene	Colorimetric/ Fluorescent	Cr^{3+}	MeOH– HEPES buffer solution	1:1	1.15 µM	Cell Imaging studies.	31
R19	Benzothizole	Fluorogenic	Hg^{2+}	THF – H_2O	-	0.59 nM	Bioimaging	32
R20	Benzothizole	Fluorogenic	Al^{3+}	DMF– H_2O	1:1	0.50 nM	Water sample, logic gate & bioimaging	33
R21	Benzothizole	Chromogenic and Fluorogenic	Al^{3+}	CH_3OH/H_2O	1:1	0.673 nM	Blood-cell imaging	34
R22	Naphthalene	Fluorogenic	Al(III)	-	1:1	-	-	35
R23	Naphthalene	Fluorogenic	Al(III)	Aqueous solution	1:1	0.43 µM	-	36
R24	Naphthalimide	Chromogenic and Fluorogenic	Al^{3+} & F^-	CH_3CN/ H_2O	-	75 µM	-	37
R25	Phenanthrenequinone	Fluorogenic	Al^{3+}	Acetonitrile	1:1	0.5 nM	-	38
R26	Schiff base	Fluorogenic	Al^{3+}	Ethanol	1:2	10.3 nM	Bioimaging	39
R27	Schiff base	Fluorogenic	Al^{3+}	Ethanol	1:1	2.59 µM	-	40
R28	Schiff base	Colorimetric & Fluorogenic	Al^{3+}	DMSO-H_2O	1:1	82 nM	Test strips & Bioimaging	41
R29	Schiff base	Fluorogenic	Al^{3+}	Methanol	1:1	5.48 nM	-	42
R30	Schiff base	Fluorogenic	Al^{3+}	Ethanol	1:1	9.27 µM	Bioimaging	43

3. Conclusions

The latest progress in identifying trivalent analytes with organic chromogenic and fluorogenic probes marks a substantial step forward in meeting the urgent demand for precise and selective detection techniques across diverse fields. This review has outlined the methods utilized in crafting probes customized for trivalent species, underscoring the vital structural elements and functional groups that bolster their ability to recognize these analytes.

Moving forward, it is essential to continue research endeavors aimed at improving the sensitivity, selectivity, and versatility of these probes to broaden their usefulness in practical situations. Future investigations might delve into novel molecular structures and refine probe designs using logical optimization approaches. Furthermore, integrating advanced sensing technologies like microfluidic devices and nanomaterial-based systems could expedite the creation of portable and high-throughput detection methods for trivalent analytes.

Competing Interests

The authors declare that they have no competing interests.

References

1. Wu D., Sedgwick A.C., Gunnlaugsson T., Akkaya E.U., Yoon J., James T.D. (**2017**) Fluorescent chemosensors: the past, present and future. *Chem. Soc. Rev*. 46, 7105-7123. https://doi.org/10.1039/C7CS00240H.
2. Upadhyay S., Singh A., Sinha R., Omer S., Negi K. (**2019**) Colorimetric chemosensors for d-metal ions: A review in the past, present and future prospect. *J. Mol. Strut.* 1193, 89-102. https://doi.org/10.1016/j.molstruc.2019.05.007.
3. Fukuhara G. (**2020**) Analytical supramolecular chemistry: Colorimetric and fluorimetric chemosensors, *J. Photochem. Photobiol. C: Photochem. Rev*. 42, 100340. https://doi.org/10.1016/j.jphotochemrev.2020.100340.
4. Alharbi K.H. (**2023**) A Review on Organic Colorimetric and Fluorescent Chemosensors for the Detection of Zn(II) Ions, *Anal. Chem*. 53, 1472-1488. https://doi.org/10.1080/10408347.2022.2033611.
5. Khan S., Chen X., Almahri A., Allehyani E.S., Alhumaydhi F.A., Ibrahim M.M., Ali S. (**2021**) Recent developments in fluorescent and colorimetric chemosensors based on schiff bases for metallic cations detection: A review, *J. Environ. Chem. Eng*. 9, 106381. https://doi.org/10.1016/j.jece.2021.106381.
6. Mohan B., Noushija M.K., Shanmugaraja S. (**2022**) Amino-1,8-naphthalimide-based fluorescent chemosensors for Zn(II) ion, *Tetrahedron Lett*. 109, 154155. https://doi.org/10.1016/j.tetlet.2022.154155.
7. Khan S., Chen X., Almahri A., Allehyani E. S., Alhumaydhi F. A., Ibrahim M. M., Ali A. (2021) Recent developments in fluorescent and colorimetric chemosensors based on schiff bases for metallic cations detection: A review, *J. Environ. Chem. Engg*. 9, 106381. https://doi.org/10.1016/j.jece.2021.106381.
8. Prabakaran G., Immanuel David C., Nandhakumar R. (**2023**) A review on pyrene based chemosensors for the specific detection on d-transition metal ions and their various applications, *J. Environ. Che. Eng.* 11, 109701. https://doi.org/10.1016/j.jece.2023.109701.
9. Liu X., Wang Y., Liu J., Tian J., Fei X. (**2023**) A high performance 2-hydroxynaphthalene acylhydrazone fluorescent chemosensor for detection of Al^{3+} ions through ESIPT and PET signalling mechanism, *J. Cluster. Sci*. 34, 813–822. https://doi.org/10.1007/s10876-022-02258-x.
10. Sivaraman G., Iniya M., Anand T., Kotla N. G., Sunnapu O., Singaravadivel S., Gulyan A., Chellappa D. (**2018**) Chemically diverse small molecule fluorescent chemosensors for copper ion. *Coor. Chem. Rev*. 357, 50-104. https://doi.org/10.1016/j.ccr.2017.11.020.
11. Woliński P., Kącka-Zych A., Wróblewska A., Wielgus E., Dolot R., Jasiński R. (**2023**) Fully Selective Synthesis of Spirocyclic-1,2-oxazine N Oxides via Non-Catalysed Hetero Diels-Alder Reactions with the Participation of Cyanofunctionalysed Conjugated Nitroalkenes, *Molecules.* 28, 4586. https://doi.org/10.3390/molecules28124586.
12. Kula K., Łapczuk A., Sadowski M., Kras J., Zawadzińska K., Demchuk O.M., Gaurav G.K., Wróblewska A., Jasiński R. (**2022**) On the Question of the Formation of Nitro-Functionalized 2,4-Pyrazole Analogs on the Basis of Nitrylimine Molecular Systems and 3,3,3-Trichloro-1-Nitroprop-1-Ene, *Molecules*. 27, 8409. https://doi.org/10.3390/molecules27238409.
13. Zawadzińska K., Gadocha Z., Pabian K., Wróblewska A., Wielgus E., Jasiński R. (**2022**) The First Examples of [3+2] Cycloadditions with the Participation of (*E*)-3,3,3-Tribromo-1-Nitroprop-1-Ene. *Materials*. 15, 7584. https://doi.org/10.3390/ma15217584.
14. Kuzu B., Tan M., Ekmekci Z., Menges N. (**2017**) A novel fluorescent sensor based on imidazole derivative for Fe^{3+} ions, *J. Lumin*. 192, 1096-1103. https://doi.org/10.1016/j.jlumin.2017.08.057.
15. Prakash S.M., Jayamoorthy K., Srinivasan N., Dhanalekshmi K.I. (**2016**) Fluorescence tuning of 2-(1H-Benzimidazol-2-yl)phenol - ESIPT process, *J. Lumin*. 172, 304-308. http://dx.doi.org/10.1016/j.jlumin.2015.12.009.

16. Zhang B., Liu H., Wu F., Hao G., Chen Y., Tan C., Tan Y., Jiang Y. (**2017**) A dual-response quinoline-based fluorescent sensor for the detection of Copper (II) and Iron(III) ions in aqueous medium, *Sens. Actuators B: Chem*. 243, 765-774. https://doi.org/10.1016/j.snb.2016.12.067.
17. Wang W., Wei J., Liu H., Liu Q., Gao Y. (**2017**) A novel colorimetric chemosensor based on quinoline for the sequential detection of Fe^{3+} and PPi in aqueous solution, *Tetrahedron Lett*. 58, 1025-1029. http://dx.doi.org/10.1016/j.tetlet.2017.01.010.
18. Wang Z., Wang H., Meng T., Hao E., Jiao L. (**2017**) Synthetically simple, click-generated quinoline-based Fe^{3+} sensors, *Methods Appl. Fluoresc*. 5, 024015. https://doi.org/10.1088/2050-6120/aa7170.
19. Lashgari N., Badiei A., Ziarani G.M. (**2016**) A fluorescent sensor for Al(III) and colorimetric sensor for Fe(III) and Fe(II) based on a novel 8-hydroxyquinoline derivative, *J Fluoresc*. 26, 1885–1894. http://dx.doi.org/10.1007/s10895-016-1883-3.
20. Madhu P., Sivakumar P. (**2019**) Selective and sensitive detection of Fe^{3+} ions using quinoline-based fluorescent chemosensor: Experimental and DFT study, *J. Mol. Struc*. 1193, 378-385. https://doi.org/10.1016/j.molstruc.2019.05.044.
21. Hao E., Meng T., Zhang M., Pang W., Zhou Y., Jiao L. (**2011**) Solvent dependent fluorescent properties of a 1,2,3-triazole linked 8-hydroxyquinoline chemosensor: tunable detection from Zinc(II) to Iron(III) in the CH_3CN/H_2O System, *J. Phys. Chem. A*. 115, 8234–8241. http://dx.doi.org/10.1021/jp202700s.
22. Aouina A., Oloyede H.O., Akong R.A., Abdelhak J., Gorls H., Plass W., Eseola A.O. (**2021**) Molecular variation and fluorescent turn-on detection of chromium(III) by three ESIPT-reactive 2,2'-(1,4-phenylenebis (5-phenyl-1H-imidazole-4,2-diyl))diphenols, *J. Photochem. Photobiol. A*. 406, 113006. https://doi.org/10.1016/j.jphotochem.2020.113006.
23. Kolcu F., Erdener D., Kaya I. (**2020**) A Schiff base based on triphenylamine and thiophene moieties as a fluorescent sensor for Cr (III) ions: Synthesis, characterization and fluorescent applications, *Inorganica Chimica Acta*. 509, 119676. https://doi.org/10.1016/j.ica.2020.119676.
24. Chalmardi G.B., Tajbakhsh M., Hasani N., Bekhradnia A. (**2018**) A new Schiff-base as fluorescent chemosensor for selective detection of Cr^{3+}: An experimental and theoretical study, *Tetrahedron*. 74, 2251-2260. https://doi.org/10.1016/j.tet.2018.03.046.
25. Zhang M., Gong L., Sun C., Li W., Chang Z., Qi D. (**2019**) A new fluorescent-colorimetric chemosensor based on a Schiff base for detecting Cr^{3+}, Cu^{2+}, Fe^{3+} and Al^{3+} ions, *Spectrochimica Acta Part A*. 214, 7-13. https://doi.org/10.1016/j.saa.2019.01.089.
26. Vijayakumar P., Dhineshkumar E., Doss M.A., Negar S.N., Renganathan R. (**2021**) Novel schiff base synthesis of E-N-(1-(1H-phenothiazin-2yl)-ethylidene)-3-((E)-(2-phenyl hydrzono) methyl) aniline ''Turn-on"fluorescent chemosensor for sensitivity and selectivity of detetion of Cr^{3+} and Pb^{2+} ions, *Mat Today: Pro*. 42, 1050-1064. https://doi.org/10.1016/j.matpr.2020.12.124.
27. Chandra R., Manna A.K., Sahu M., Rout K., Patra G.K. (**2020**) Simple salicylaldimine functionalized dipodal bis Schiff base chromogenic and fluorogenic chemosensors for selective and sensitive detection of Al^{3+} and Cr^{3+}, *Inorganica Chimica Acta*. 499, 119192. https://doi.org/10.1016/j.ica.2019.119192.
28. Dhineshkumar E., Iyappan M., Anbuselvan C. (**2020**) A novel dual chemosensor for selective heavy metal ions Al^{3+}, Cr^{3+} and its applicable cytotoxic activity, HepG2 living cell images and theoretical studies, *J .molstruc*. 15, 1128033. https://doi.org/10.1016/j.molstruc.2020.128033.
29. Hu T., Wang L., Li J., Zhao, Y., Cheng J., Li W., Chang Z., Sun C. (**2021**) A new fluorescent sensor L based on fluorene-naphthalene Schiff base for recognition of Al^{3+} and Cr^{3+}, *Inorganica Chimica Acta*. 524, 120421. https://doi.org/10.1016/j.ica.2021.120421.
30. Mukherjee S., Betal S., Chattopadhyay A.P. (**2020**) Dual sensing and synchronous fluorescence spectroscopic monitoring of $Cr^{3+}$and Al^{3+} using a luminescent Schiff base: Extraction and DFT studies, *Spectrochimica Acta Part A: Mole and Biomole Spec*. 228, 117837. https://doi.org/10.1016/j.saa.2019.117837.
31. Mahata S., Janani G., Mandal B.B., Manivannan V. (**2021**) A coumarin based visual and fluorometric probe for selective detection of Al(III), Cr(III) and Fe(III) ions through "turn-on" response and its biological application, *J Photochem and Photobio A: Chem*. 417, 13340. https://doi.org/10.1016/j.jphotochem.2021.113340.
32. Zeng S., Li S-J., Sun X-J., Li M-Q., Xing Z-Y., Li J-L. (**2019**) A benzothiazole-based chemosensor for significant fluorescent turn-on and ratiometric detection of Al^{3+} and its application in cell imaging, *Inorganica Chim Acta*. 486, 654-662. https://doi.org/10.1016/j.ica.2018.11.042.
33. Zeng S., Li S-J., Liu T-T., Sun X-J., Xing Z-Y. (**2019**) A significant fluorescent "turn-on" chemosensor for Al^{3+} detection and application in real sample, logic gate and bioimaging, *Inorganica Chim Acta*. 495, 118962. https://doi.org/10.1016/j.ica.2019.118962.
34. Goswami S., Das S., Aich K., Ghoshal K., Quah C. K., Bhattacharyya M., Fun H. K. (**2015**) ESIPT and CHEF based highly sensitive and selective ratiometric sensor for Al^{3+} with imaging in human blood cell, *New J. Chem*. 39, 8582-8587. https://doi.org/10.1039/C5NJ01468A.
35. Liu L., Sun B., Ding R., Mao Y., Di M. (**2020**) Al^{3+} regulated competition between TICT and ESIPT of a chemosensor, *J Lumin*. 228, 117657. https://doi.org/10.1016/j.jlumin.2020.117657.

36. Yue X-l., Wang Z-Q., Li C-R., Yang Z-Y. (**2017**) Naphthalene-derived Al^{3+}-selective fluorescent chemosensor based on PET and ESIPT in aqueous solution, *Tetrahedron Lett*. 58, 4532-4537. https://doi.org/10.1016/j.tetlet.2017.10.044.
37. Kumar G., Singh I., Goel R., Paul K., Luxami V. (**2021**) Dual-channel ratiometric recognition of Al^{3+} and F^- ions through an ESIPT-ESICT signalling mechanism, S*pectrochim. Acta - A: Mol. Biomol*. 247, 119112. https://doi.org/10.1016/j.saa.2020.119112.
38. Sinha S., Chowdhury B., Ghosh P. (**2016**) A highly sensitive ESIPT-based ratiometric fluorescence sensor for selective detection of Al^{3+}, *Inorg. Chem*. 55, 9212–9220. https://doi.org/10.1021/acs.inorgchem.6b01170.
39. Li Z., Liu C., Wang J., Wang S., Xiao L., Jing X. (**2019**) A selective diaminomaleonitrile-based dual channel emissive probe for Al^{3+} and its application in living cell imaging, Spectrochim*. Acta - A: Mol. Biomol*. 212, 349-355. https://doi.org/10.1016/j.saa.2019.01.031.
40. Kolcu F., Kaya I. (**2022**) Carbazole-based Schiff base: A sensitive fluorescent 'turn-on' chemosensor for recognition of Al(III) ions in aqueous-alcohol media, *Arabian. J. Chem*. 15, 103935. https://doi.org/10.1016/j.arabjc.2022.103935.
41. Xu H., Chen W., Ju L., Lu H. (**2021**) A purine based fluorescent chemosensor for the selective and sole detection of Al^{3+} and its practical applications in test strips and bio-imaging, *Spectrochim. Acta - A: Mol. Biomol*. 247, 119074. https://doi.org/10.1016/j.saa.2020.119074.
42. Akong R.A., Gorls H., Woods J.A. O., Plass W., Eseola A.O. (**2021**) ESIPT-inspired fluorescent turn-on sensitivity towards aluminium(III) detection by derivatives of O- and S-bridged bis-(phenol-imine) molecules, *Res. Chem*. 3, 100236. https://doi.org/10.1016/j.rechem.2021.100236.
43. Das B., Dey S., Maiti G.P., bhattacharjee A., Dhara A., Jana A. (**2018**) Hydrazinopyrimidine derived novel Al^{3+} chemosensor: molecular logic gate and biological applications, *New J. Chem*. 42, 9424-9435. https://doi.org/10.1039/C7NJ05095J.